Environ. Sci. Technol. **2003**, *37*, 561−568

Kinetic Modeling of TiO_2-Catalyzed Photodegradation of Trace Levels of Microcystin-LR

ANDREW J. FEITZ AND T. DAVID WAITE*
School of Civil and Environmental Engineering, University of New South Wales, Sydney, New South Wales 2052, Australia

A kinetic model has been developed to investigate the relative importance of major pathways for the photocatalytic degradation of trace levels of the cyanobacterial toxin microcystin-LR (MLR) in solutions containing a complex suite of dissolved organic matter and to test the sensitivity of MLR degradation to rate constants of the key processes. The kinetic model incorporates adsorption of the trace contaminant, other organics and oxygen on the particle surface, surface reactions between adsorbed radical and nonradical species, desorption of surface radical species, solution phase radical reactions, and radical termination pathways. Under conditions where the contaminant adsorbs strongly to semiconductor surface sites, rapid degradation is observed, and a primary degradation step appears to involve reaction between surface-located long-lived organic radicals (formed from hydroxyl radical scavenging by the bulk organic) and adsorbed trace contaminant. MLR degradation is relatively insensitive to changes in light intensity under these strongly adsorbing conditions but highly dependent under weakly adsorbing conditions and when solution phase degradation is important. While not verified independently, desorption of surface bound superoxide appears to lead to the production of organic peroxyl radicals through reaction of superoxide with the bulk organic. These solution phase organic peroxyl radicals are highly reactive and appear to be the primary source of trace contaminant degradation under conditions where the trace contaminant shows no observable adsorption and surface degradation is negligible. Under alkaline conditions, adsorption of carbonate onto the particle surface results in scavenging of surface hydroxyl radicals to form surface carbonate radicals that rapidly quench surface bound superoxide. This prevents organic peroxyl production, the primary agent of solution-phase trace contaminant degradation.

Introduction

Recent work assessing the applicability of photocatalytic degradation to the cyanobacterial toxin microcystin-LR (MLR) has demonstrated that the toxin is highly susceptible to photooxidation (*1*−*3*) with partial degradation substantially reducing the toxicity of the compound (*4*). Complications arise, however, when the toxin is a trace contaminant in the presence of a wide range of other constituents, many of which are present at concentrations orders of magnitude higher than the contaminant. We have recently reported detailed TiO_2-catalyzed photodegradation studies in one such composite system involving the breakdown of a cyanobacterial toxin (MLR) in the presence of a large excess of ill-defined cyanobacterial exudate (*1*). The initial rate of toxin degradation was strongly pH dependent, mirrored by the pH dependence of toxin adsorption to TiO_2, and highly concentration dependent. A simple surface complexation model adequately describes the effect of pH on microcystin-LR (MLR) adsorption to TiO_2 (*1*), and a conceptual model was developed to describe degradation kinetics (*5*). While the conceptual model adequately describes degradation behavior both at low and high pH for a fixed concentration, the model poorly predicted the effects on increasing concentration for low and high pH scenarios. The greater extent of predicted than observed degradation is attributed to the presence of additional concentration dependent pathways for deactivation of exudate free radicals that are unaccounted for in the relatively simple system proposed previously (*5*). The model described in this paper serves to include the major deactivation pathways of exudate free radicals and, in so doing, provide insight into the dominant pathways for photocatalytic degradation of trace levels of MLR within a natural matrix of dissolved organic matter (DOM).

Experimental Section

As described in detail by Feitz et al. (*1*) near-UV lamp and 1 h dark adsorption experiments were performed in a water-jacketed borosilicate glass vessel incorporating a quartz window for catalyst irradiation. Near-UV light was supplied by a 100 W high-pressure Hg arc lamp with a 365 nm bandpass filter. Total irradiation was determined by ferrioxalate actinometry and found to be 1600 μmol·m^{-2}·s^{-1}. Titanium dioxide suspensions of 1 g·L^{-1} were used for all experiments and consisted of a cyanobacerial extract diluted to the desired concentration with Milli-Q water and Tioxide Australia TiO_2 (principally anatase) with an average crystal size of approximately 100 nm and a surface area of 10 m^2·g^{-1}. The temperature of the reaction vessel was kept constant at 20.0 ± 1.0 °C using a recirculating refrigerated water bath and pH was adjusted with 5% HNO_3 or 0.1 M NaOH depending on the required pH before injection of the MLR/DOM mixture. Detailed adsorption and reaction rate studies were undertaken at pH 8.6 (adjusted by addition of $NaHCO_3$ to $10^{-2.8}$M) and pH 3.5 in a 0.01 M $NaNO_3$ background electrolyte.

The dissolved organic material used in the study was cyanobacterial extract separated from a highly toxic cyanobacterial bloom of *Microcystis aeruginosa* and contained 73 μM microcystin-LR and a dissolved organic carbon content of 2200 μg/mL. MLR consists of a cyclic arrangement of seven amino acids with three main functional groups imparting the molecule's acid−base functionality—two acidic groups (erythro-*b*-methyl aspartic acid and D-glutamic acid) and a basic group (L-arginine) (Figure 1). The organic matter present in addition to MLR was presumably a complex mixture of exudate compounds (including chlorophyll *a*, β-carotene, proteins, and fatty acids (*6*)). Time zero was the time of injection of the MLR/exudate mixture into the reactor after lamp warm-up (approximately 30 min) and addition and initial rapid mixing of TiO_2 (approximately 5 s before addition of the MLR/exudate mixture). High performance liquid chromatography (Hewlett-Packard 1100) was used to determine MLR concentrations in both adsorption and photodegradation studies, and a Shimadzu 5000A TOC analyzer was used to determine the extent of DOM adsorption. Details of these techniques are given elsewhere (*1*). Note that degradation of the toxin by direct photolysis has previously been shown to be minimal (*1*).

* Corresponding author phone: +61-2-9385 5060; fax: +61-2-9385 6139; e-mail: d.waite@unsw.edu.au.

10.1021/es0256010 CCC: $25.00
Published on Web 12/21/2002

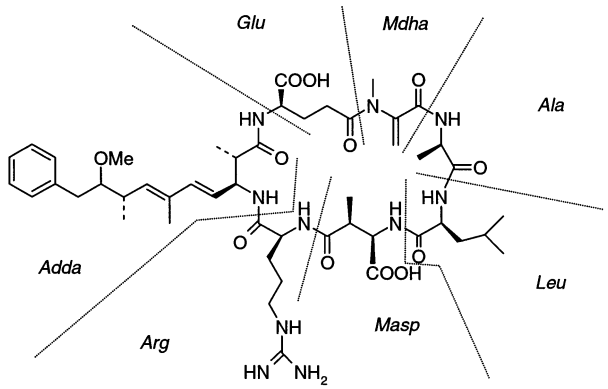

FIGURE 1. Structure of the blue-green algal toxin microcystin-LR. Besides the two variable L-amino acids, leucine and arginine, the microcystin contains three D-amino acids (glutamic acid, alanine, and methylaspartic acid) and two unusual amino acids, *N*-methyldehydroalanine (Mdha) and 3-amino-9-methoxy-2,6,8-trimethyl-10-phenyldeca-4,6-dienoic acid (Adda) (reproduced from ref *32*).

Numerical Modeling. The photocatalytic degradation of $MLRH^-$ in an aqueous−organic matrix was modeled numerically using the program ACUCHEM (*7*). The program uses implicit, variable order, linear multivalue integration methods with the appropriate method selected by the program to minimize computational effort (*8*). The integration time step is automatically determined by the program based on the integration tolerance specified by the user, which was 0.001 in our case. Optimization of unknown or poorly defined parameters was undertaken by visual inspection of the model curve fitted to data. To examine the sensitivity of the model to variation in a particular rate constant, the square of residuals between the original (control) model output and the perturbed model output was calculated. The sum of squares of the residuals (SSR) was calculated as follows, where m_i and p_i represent the predicted $MLRH^-$ concentrations in the control and perturbed models respectively at each data point:

$$\mathrm{SSR} = \sum \frac{(m_i - p_i)^2}{m_i}$$

Sensitivity analysis was undertaken by varying the rate constant for a particular reaction, while the other rate constants were unchanged. This approach assumes that the rate constants in the original model are close to the correct value, since a change in one of the rate constants may affect the sensitivity of the model to a change in another of the rate constants. The change in model output was considered by perturbing each rate constant by an order of magnitude (both increase and decrease).

Results and Discussion

Surface-Mediated Degradation (Part A). The model used in this study is an extension of an approach proposed by Waite et al. (*5*) to account for the removal of MLR as a trace contaminant from a natural organic-TiO_2 suspension but incorporates additional radical degradation and termination pathways. Quantitative kinetic modeling of the various species is achieved by first using a surface complexation model to determine equilibrium constants for adsorption of both the negatively charged MLR (microcystin) species (referred to as $MLRH^-$) and generic "bulk organic" $RR''CH_2^-$ to TiO_2 (*1*). These values are then incorporated together with the degradation rate constants into the rate modeling software ACUCHEM (*7*). Physical properties of the experimental system adopted for use in the model include a TiOH site density of 4×10^{-5} M (*1*), fixing $MLRH^-$ at 3 wt % $RR''CH_2^-$, and assuming an average molecular weight of $RR''CH_2^-$ of 1000 g·gmol^{-1}. Solution phase rate constants given below have been compiled from various sources (*9*−*12*), and for $MLRH^-$ and $RR''CH_2^-$, where no rate constants exist, the order of magnitude for the constants is estimated from like reactions with peptides and proteins.

The model (see Table 1) is comprised of reversible adsorption reactions between MLRH-, $RR''CH_2^-$, and O_2 and the surface of TiO_2 (eqs 1−3), generation of primary radicals species (eqs 4−8), desorption of superoxide into solution (eq 9), and subsequent radical termination pathways for the superoxide species (eqs 10−13). Desorption of superoxide into solution during photocatalysis has been recently confirmed (*17*, *18*). Surface hydroxyl radicals are generated at the holes (eq 14) and then react with adsorbed organic species (eqs 15−17) to form surface organic alkyl radicals. These organic alkyl radicals may either react with the adsorbed $MLRH^-$ (eq 17), cycle with the bulk organic, or undergo a series of radical termination steps (eqs 18−21). For a full justification of the rate constants and reactions adopted in the model, see the Supporting Information. Note that the purpose of this model is not to replicate the unusual degradation behavior of the microcystin-LR in a complex organic matrix but to investigate the relative importance of possible degradation pathways under various conditions and to use the model to test the sensitivity of MLR degradation to rate constants of the key processes.

An important aspect of the model is the time dependent adsorption of the organics to the particle surface. The criteria used to determine the forward rate constant for $MLRH^-$ adsorption at pH 3.5 is simply that the initial rate of adsorption is assumed no faster than the observed initial rate of degradation. This is under the limitation of the given conditional stability constant and the extent of adsorption observed over the course of 1 h. The pH dependent tendency of the toxin and, to a far lesser degree, exudate, to adsorb to the semiconductor surface was modeled by varying the conditional formation constants for toxin and exudate surface complexes. This was achieved by setting the forward reaction rates (k_f) for formation of these surface complexes at fixed values and varying the back (desorption) reaction rates (k_b). Since $MLRH^-$ adsorption is strongly pH dependent (eq 1) the back desorption reaction rate at pH 8.6 is approximately 10^5 times greater than that at pH 3.5. No time dependent data on the adsorption of $RR''CH_2^-$ onto TiO_2 (eq 2) is available so the forward adsorption rate is assumed similar in magnitude to that for $MLRH^-$ (i.e. 10 s^{-1}), and the back desorption rate constant is then calculated from the observed conditional stability constant. This is calculated for each concentration and pH. Table 2 lists adsorption rate constants for different MLR and $RR''CH_2^-$ concentrations at pH 3.5 and 8.6.

As can be seen in Figure 2, the model based on surface-mediated degradation of $MLRH^-$ (via eqs 15 and 17) provides a good description of the data. Order of magnitude perturbation of the rate constants used in this model (Figure 3) suggests that the rates of adsorption/desorption of $MLRH^-$ to the particles surface are the key determinants of degradation rate followed by the rates of oxygen adsorption/desorption to the particles surface. Note that variation of the rate constants for adsorption reactions involves increasing or decreasing both the adsorption and desorption rate constants simultaneously to maintain the same stability constant. As an initial guide, we have assumed that the rate of superoxide adsorption or desorption is similar to that for oxygen, although at this stage of the modeling inclusion or omission of this radical pathway has no effect on model predictions.

TABLE 1. Surface-Mediated Degradation (Part A) Reaction Sequence[a]

eq no.	reaction	rate or complexation constant	ref[b]
1	$>TiOH + MLRH^- + H \leftrightarrow >TiMLRH + H_2O$	logK = 8	(*1*)
2	$>TiOH + RR''CH_2^- \leftrightarrow TiRR''CH_2 + OH^-$	$\log K_c \sim 4$	(*5*)
3	$>TiOH + O_2 \leftrightarrow >TiOH:O_2$	LogK ~ 4	(*15*)
4	$>TiOH + h\nu \leftrightarrow >TiOH + h^+_{vb} + e^-_{cb}$		H
5	$\Phi I \rightarrow h^+_{vb}$	$k = 4 \times 10^{-6}\ M^{-1}\ s^{-1}$	H
6	$\Phi I \rightarrow e^-_{cb}$	$k = 4 \times 10^{-6}\ M^{-1} s^{-1}$	H
7	$>TiOH + h^+_{vb} + e^-_{cb} \leftrightarrow >TiOH$ + heat/light	$k = 4.6 \times 10^{23}\ M^{-1} s^{-1}$	(*16*)
8	$>TiOH:\ O_2 + e^-_{cb} \leftrightarrow >TiOH:\ O_2^{\bullet -}$	$k = 1.9 \times 10^{10}\ M^{-1} s^{-1}$	(*16*)
9	$> TiOH:\ O_2^{\bullet -} \leftrightarrow > TiOH + O_2^{\bullet -}$	LogK ~ 4	L
10	$HO_2^{\bullet} + O_2^{\bullet -} \rightarrow HO_2^- + O_2$	$k = 9.7 \times 10^7\ M^{-1} s^{-1}$	(*18*)
11	$HO_2^{\bullet} + HO_2^{\bullet} \rightarrow H_2O_2 + O_2$	$k = 8.3 \times 10^5\ M^{-1} s^{-1}$	(*18*)
12	$O_2^{\bullet -} + H^+ \leftrightarrow HO_2^{\bullet}$	Logk = 4.8	(*19*)
13	$HO_2^- + H^+ \rightarrow H_2O_2$	Logk = 11.7	(*19*)
14	$> TiOH + h^+_{vb} \rightarrow > TiOH^{\bullet +}$	$k = 2 \times 10^{12}\ M^{-1} s^{-1}$	(*16*)
15	$>TiOH^{\bullet +} + >TiMLRH \rightarrow >TiOH_2^+ + TiMLR^{\bullet}$	$k = 10^9\ M^{-1} s^{-1}$	H
16	$>TiOH^{\bullet +} + > TiRR''CH_2 \rightarrow >TiOH_2^+ + > TiRR''CH^{\bullet}$	$k = 10^9\ M^{-1} s^{-1}$	H
17	$> TiRR''CH^{\bullet} + TiMLRH \rightarrow TiRR''CH_2 + > TiMLR^{\bullet}$	$k = 10^8\ M^{-1} s^{-1}$	H
18	$> TiRR''CH^{\bullet} + > TiRR''CH^{\bullet} \rightarrow >TiRR''CH^- + TiRR''CH^+$	$k = 10^9\ M^{-1} s^{-1}$	M
19	$> TiOH:\ O_2^{\bullet -} + > TiRR''CH^{\bullet} \rightarrow >TiOH:\ O_2 + > TiRR''CH^-$	$k = 10^7\ M^{-1} s^{-1}$	M
20	$> TiMLR^{\bullet} + > TiRR''CH^{\bullet} \rightarrow > TiMLR^- + >TiRRCH^+$	$k = 10^9\ M^{-1} s^{-1}$	M
21	$> TiMLR^{\bullet} + >TiOH:O_2^{\bullet -} \rightarrow > TiMLR^- + >TiOH:O_2$	$k = 10^7\ M^{-1} s^{-1}$	M

[a] Refer to Supporting Information for justification of rate constant estimates. [b] H = high confidence − rate constant estimate correct within 1 order of magnitude. M = medium confidence − rate constant estimate may be greater than 1 order of magnitude. L = low confidence/unknown.

TABLE 2. Determined Adsorption/Desorption (Back) Rate Constants for Dark Adsorption of $MLRH^-$ and $RR'CH_2^-$ onto TiO_2[a]

	pH 3.5				pH 8.6			
	MLR		TOC		MLR		TOC	
MLR_o (nM)	k_f (s^{-1})	k_b (s^{-1})	k_f (s^{-1})	k_b (s^{-1})	k_f (s^{-1})	k_b (s^{-1})	k_f (s^{-1})	k_b (s^{-1})
~450	3	1.2×10^{-4}	10	2.7×10^{-3}	3	1.2×10^{1}	10	12×10^{-3}
~350	4	1.6×10^{-4}	10	2.4×10^{-3}	4	1.6×10^{1}	10	8×10^{-3}
~240	5	2×10^{-4}	10	1.6×10^{-3}	5	2×10^{1}	10	3.3×10^{-3}
120	40	1.6×10^{-3}	10	1.1×10^{-3}	40	1.6×10^{2}	10	2.8×10^{-3}
85	50	2×10^{-3}	10	1.0×10^{-3}	50	2×10^{2}	10	2.8×10^{-3}
60	50	2×10^{-3}	10	1.0×10^{-3}				

[a] The $\log K_c$ values for TOC gives observed dark adsorption removal over a 1 h period. $\log K_c$ for MLR is based on eq 1, and k_f values for MLR at low pH are based on observed initial removal rates.

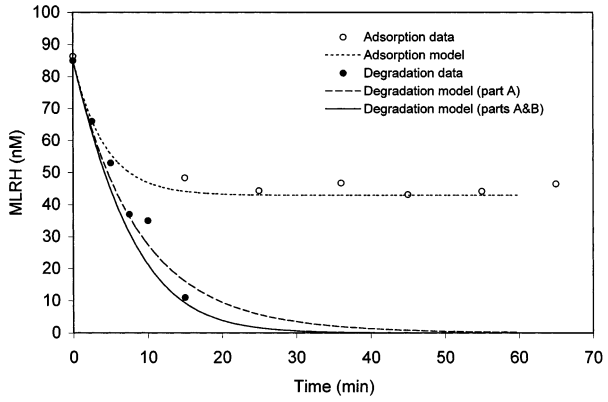

FIGURE 2. Loss of microcystin-LR from solution at pH 3.5 and low concentration. Ionic strength of 0.01 M and TiO_2 loading of 1 g·L^{-1}; "degradation model (part A)" refers to the surface only degradation model; "degradation model (parts A and B)" incorporates both surface and solution degradation components; adsorption model excludes light based reactions.

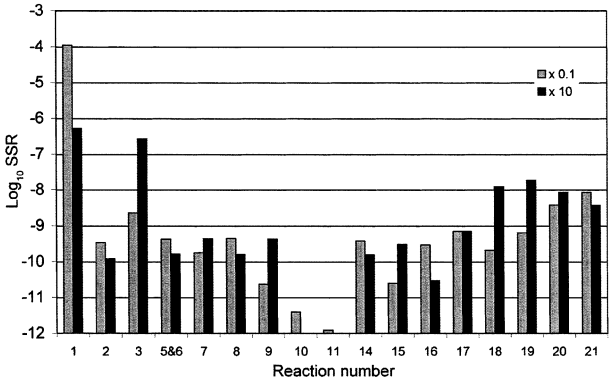

FIGURE 3. Log sum of squares of the residuals (log SSR) for 1 order of magnitude (increase and decrease) perturbation of each rate constant for degradation model (part A: surface degradation) at pH 3.5, C_o = 85 nM, I = 0.01 M, and TiO_2 = 1 g·L^{-1}.

To assist in placing the extent of change induced in predicted $MLRH^-$ degradation rates on perturbation in selected rate constants in perspective, we show the effects of order of magnitude change in rate constants for eqs 1 and 3 in Figure 4 (parts a and b), respectively. A decrease in rate of uptake of $MLRH^-$ onto the titania surface from the optimal value by an order of magnitude is seen to result in a significant decrease in the rate of $MLRH^-$ degradation (as quantified by a logSSR = −4.0) compared to the optimal model, while a 10-fold increase in adsorption rate also results in a sizable departure from the optimal model prediction (as quantified by a logSSR = −6.3). Similarly, an order of magnitude decrease

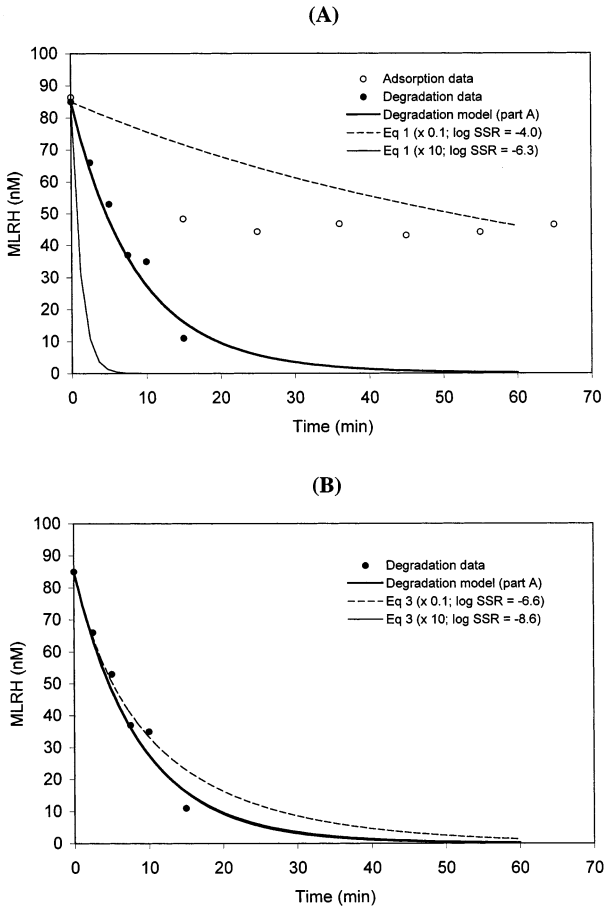

FIGURE 4. Example perturbation for $MLRH^-$ adsorption (eq 1) (a) and oxygen adsorption (eq 3) (b) for the degradation model (part A) at pH 3.5, $C_0 = 85$ nM, $I = 0.01$ M, and $TiO_2 = 1$ gm·L^{-1}. Note that it is not possible to visually detect the order of magnitude perturbation increase for eq 3 ($\times$10; logSSR $= -8.6$).

in the rate of oxygen adsorption to the titania surface results in a small but distinct departure from the optimal model prediction (with a logSSR $= -6.6$), while an order of magnitude increase in oxygen adsorption rate has no noticeable effect on model prediction (logSSR $= -8.6$).

Under conditions where there is fast initial toxin adsorption, 10-fold changes in the light intensity (and hence h^+ and e^- production; eqs 5 and 6) has minimal effect on the overall degradation profile of the trace organic (Figure 3; eqs 5 and 6). This surprising result is only observed under conditions where surface-mediated toxin degradation dominates and confirms that adsorption kinetics rather than light intensity is rate limiting. The expected impact of changes in light intensity on rate of toxin degradation is observed under conditions where both surface and solution pathways of toxin degradation are important (part B) and under conditions where toxin adsorption to the catalyst is unimportant (part C). These cases are discussed in detail below with the relatively simple surface-mediated model developed above used as a starting point for examination of toxin degradation under conditions where additional processes become important.

Addition of Solution Phase Toxin Degradation (Part B). Application of the surface only model (part A) to high concentrations of $MLRH^-$ and $RR''CH_2^-$ does not adequately predict the extent of removal of $MLRH^-$ (Figure 5). The modification of the adsorption and desorption rate constants to reflect the new levels of adsorption of $MLRH^-$ and $RR''CH_2^-$ (Table 2) ensures that the initial rate of $MLRH^-$ removal is accurately described. After a few minutes, however, the rate of $MLRH^-$ degradation increases and this is not described

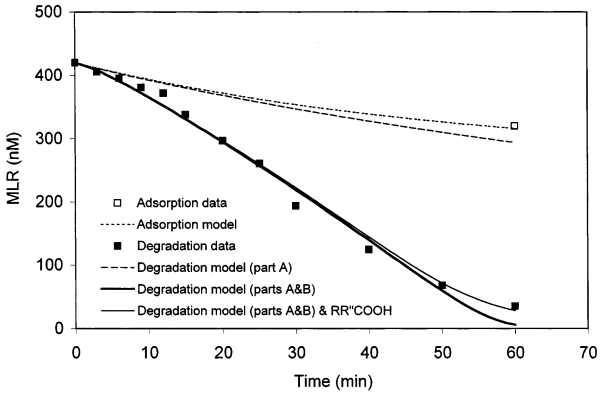

FIGURE 5. Loss of microcystin-LR from solution at pH 3.5 at high concentration. Ionic strength of 0.01 M and TiO_2 loading of 1 g·L^{-1}; "degradation model (part A)" refers to the surface only degradation model; "degradation model (parts A and B)" incorporates both surface and solution degradation components; adsorption model excludes light based reactions; "degradation model (parts A and B) and RR″COOH" incorporates both surface and solution degradation components but excludes oxygenated products from any further reactions.

by the model developed in part A. Decreasing the rate of adsorption of oxygen onto the surface to facilitate greater access for the bulk organics which sensitize $MLRH^-$ degradation (via eq 17) does not improve the model prediction significantly. Since surface effects cannot describe the degradation under high concentration conditions, it is necessary to introduce solution phase degradation pathways (Table 3).

There are essentially two mechanisms by which solution phase degradation may be initiated: (i) desorption of $O_2^{\bullet-}$ and inducement of a free radical degradation pathway through reaction of superoxide with the bulk organic and (ii) desorption of $RR''CH^{\bullet-}$ from the surface into solution (assuming that $RR''CH^{\bullet-}$ is sufficiently long-lived). Due to the presence of high levels of O_2 in solution ($\sim 10^{-4}$ M), $RR''CH^{\bullet-}$ is likely to rapidly form peroxyl radicals (eq 23) that may either undergo self-decomposition (eq 24) or propagation reactions with MLR (eq 25), bulk organic (eq 26), or terminate with $HO_2^{\bullet-}/O_2^{\bullet-}$ (eq 27).

In part A of the model, we ignored the possibility that $HO_2^{\bullet-}/O_2^{\bullet-}$ may react with solution phase MLRH or the bulk organic. There is a wide variation in rate constants for $HO_2^{\bullet-}/O_2^{\bullet-}$ reactions with peptides and proteins. The typical range is 10^2–10^6 M^{-1} s^{-1}, which is considerably less than the rate constant for the reaction with organic peroxy radicals shown in eq 25. It is therefore unlikely that the primary solution phase degradation pathway for MLRH will be via superoxide (eq 29). An important potential pathway, however, is the production of peroxyl radicals through reactions between the bulk organic and $HO_2^{\bullet-}/O_2^{\bullet-}$ as given in eq 28. Any alkyl radicals formed through interaction of the bulk organic with superoxide would be expected to rapidly react with dissolved O_2 resulting in the formation of highly reactive organic peroxyl radicals. Equations 28 and 29 are assumed to be moderately fast, and the sensitivity of this assumption is discussed below. The primary termination pathway for solution phase microcystin radicals is considered to be with superoxide as given in eq 30.

Note that solution phase degradation via hydroxyl radicals has not been considered in the model. If hydroxyl radicals do desorb from the catalysts' surface, they are unlikely to migrate far due to their high reactivity and concomitant relatively short lifetime. Degradation must take place within a few hundred atomic distances of the catalyst's surface (*28*, *29*). Cornish et al. (*30*) postulated that solution phase

TABLE 3. Addition of Solution Phase Toxin Degradation (Part B) Reactions[a]

eq no.	reaction	rate or complexation constant	ref[b]
22	$> TiRR''CH^{\bullet} + OH^{-} \rightarrow TiOH + RR''CH^{\bullet -}$		
23	$RR''CH^{\bullet -} + O_2 \rightarrow >RR''CHOO^{\bullet -}$	$k = 2 \times 10^9\ M^{-1} s^{-1}$	(*10*, *26*)
24	$RR''CHOO^{\bullet -} \rightarrow O_2^{\bullet -} + RR''CH$	$k = 10^2\ s^{-1}$	H
25	$RR''CHOO^{\bullet -} + MLRH \rightarrow RR''CHOOH + MLR^{\bullet -}$	$k = 10^8\ M^{-1} s^{-1}$	H
26	$RR''CHOO^{\bullet -} + RR''CH_2^{-} \rightarrow RR''CHOOH + RR''CH^{\bullet 2-}$	$k = 10^8\ M^{-1} s^{-1}$	H
27	$RR''CHOO^{\bullet -} + HO_2^{\bullet} \rightarrow RR''CH^{-} + O_2$	$k = 10^8\ M^{-1} s^{-1}$	M
28	$RR''CH_2^{-} + HO_2^{\bullet} \rightarrow RR''CHOOH^{\bullet -} + H_2O_2$	$k = 10^5\ M^{-1} s^{-1}$	M
29	$MLRH + HO_2^{\bullet} \rightarrow MLR^{\bullet} + H_2O_2$	$k = 10^5\ M^{-1} s^{-1}$	M
30	$MLR^{\bullet -} + HO_2^{\bullet} \rightarrow MLR + HO_2^{-}$	$k = 10^7\ M^{-1} s^{-1}$	M

[a] Refer to Supporting Information for justification of rate constant estimates. [b] H = high confidence − rate constant estimate correct within 1 order of magnitude. M = medium confidence − rate constant estimate may be greater than 1 order of magnitude. L = low confidence/unknown.

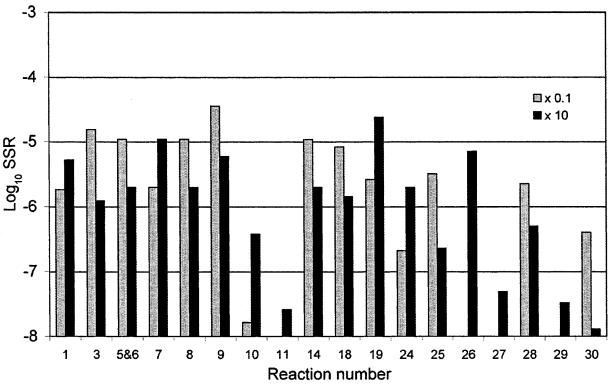

FIGURE 6. Log sum of squares of the residuals (log SSR) for 1 order of magnitude (increase and decrease) perturbation of each rate constant for degradation model (parts A and B) at pH 3.5, $C_o = 420$ nM, $I = 0.01$ M, and $TiO_2 = 1$ g·L^{-1}.

degradation of MLRH may take place via hydroxyl radicals formed through the reaction of superoxide with H_2O_2. This is considered unlikely in this case as the rate constant for reaction between $HO_2^{\bullet -}/O_2^{\bullet -}$ and H_2O_2 ranges from $10^{-4} - 3.7$ $M^{-1} s^{-1}$ (*11*) compared to approximately $10^2 - 10^6$ $M^{-1} s^{-1}$ for reactions with peptides and proteins (which are present in much greater concentrations).

Unlike the dominance of the adsorption/desorption of MLRH in part A of the model (Figure 3; eq 1), there is no single reaction that dominates $MLRH^{-}$ degradation once solution phase reactions are incorporated into the model. The desorption of $>TiOH:O_2^{\bullet -}$ (Figure 6; eq 9) and the quenching of surface radicals (Figure 6; eqs 18 and 19) appear to be particularly significant, although the production and recombination (Figure 6; eqs 5−8 and 14) of the primary oxidizing and reducing species is also critical. The rate of adsorption/desorption of MLRH and O_2 is also important (Figure 6; eqs 1 and 3) as are reactions concerning the production and termination of peroxy radicals in solution (Figure 6; eqs 24−26 and 28). This combination of reactions provides some insight into the likely major degradation pathway. It is clear that surface degradation cannot account for the lag effect apparent in Figure 5 and that the release of $O_2^{\bullet -}$ from the surface is important for initiating solution phase degradation. Release of $RR''CH^{\bullet -}$ radical from the surface into solution (eq 22) has a limited impact on the model predictions. For $>TiRR''CH^{\bullet -}$ desorption to significantly contribute to solution phase degradation, the desorption rate must be very fast ($0.4\ s^{-1}$) which in turn cannot then account for the observed lag effect (data not shown). This suggests that reactions involving $HO_2^{\bullet -}/O_2^{\bullet -}$ are intimately involved in initiating solution phase degradation. A further indication of the importance of superoxide in toxin degradation is the sensitivity of the model to reactions involving $O_2^{\bullet -}$. Equation 19, the quenching of surface $>TiOH:O_2^{\bullet -}$ with $>TiRR''CH^{\bullet -}$, reduces the opportunity for $O_2^{\bullet -}$ to desorb into solution and initiate solution phase degradation. Rapid self-quenching of the surface $>TiRR''CH^{\bullet -}$ radicals (eq 18), alternatively, results in less radicals available for the quenching of surface $>TiOH:O_2^{\bullet -}$ and hence greater $O_2^{\bullet -}$ desorption and solution phase MLRH degradation.

Faster MLRH adsorption/desorption results in greater access to surface hydroxyl radicals and therefore faster surface mediated degradation as indicated in part A. The importance of oxygen adsorption/desorption (eq 3) and the production of e^{-} and h^{+} on the surface (eqs 5−8 and 14) is linked to the production and availability of surface $>TiOH:O_2^{\bullet -}$ radicals that may desorb into solution (and which subsequently initiate solution phase degradation). Surface degradation is only the primary degradation mechanism when there is fast MLRH adsorption. The order of magnitude perturbation of all other reactions as shown in Figure 3 (and reactions not shown but with a logSSR < -8) are related to the promotion or consumption of $O_2^{\bullet -}$ and the degradation of MLRH− by $RR''CHOO^{\bullet -}$ (Figure 6; eqs 24−26 and 28). This is an important distinction from the surface mediated degradation model given in part A and indicates that adsorption of $MLRH^{-}$ is no longer the rate-limiting step under these conditions.

It therefore appears that desorption of surface $>TiOH:O_2^{\bullet -}$ radicals rather than potentially long-lived $RR''CH^{\bullet -}$ radicals is the first step in initiating solution phase degradation of the toxin. If solution phase $HO_2^{\bullet -}$ reacts equally rapidly with MLRH and the bulk organic (e.g. $10^5\ M^{-1} s^{-1}$), then the major solution phase degradation occurs via the $HO_2^{\bullet -} - RR''CH^{\bullet -} - RR''CHOO^{\bullet -} - MLRH$ pathway with the contribution from direct reaction of MLRH with $HO_2^{\bullet -}$ being comparatively minor. When the model incorporates surface (part A) and solution (part B) degradation pathways, it has the capacity to accurately describe the degradation of $MLRH^{-}$ over a wide range of concentrations and different organic adsorption conditions (Figure 7). Reapplication of the part A model but with the addition of part B reactions to the low concentration scenario results in only a slight increase in the degradation rate (Figure 2) (logSSR $= -7.2$), confirming that where adsorption of the trace contaminant is strong the major degradation pathway is via surface degradation. While the introduction of solution phase reactions has led to a more complex model compared to the "surface only" model developed in part A, slow desorption of superoxide enables lag effects to be described satisfactorily and suggests that this is a potentially important pathway for solution phase degradation under conditions where the extent of adsorption to the catalyst surface is minor or nonexistent.

Addition of Carbonate Effects at High pH (Part C). No adsorption of $MLRH^{-}$ onto TiOH was observed at pH 8.6 (*1*), yet significant degradation over a wide range of toxin concentrations is apparent (Figures 8−10). Clearly, surface

TABLE 4. Addition of Carbonate Effects at High pH (Part C) Reactions[a]

eq no.	reaction	rate or complexation constant	ref[b]
31	$> TiOH + CO_3^{2-} + H+ \rightarrow > TiCO_3^- + H_2O$	$\log K = 13$	(*30*)
32	$> TiOH^{\bullet+} + > TiCO_3^- \rightarrow > TiOH + > TiCO_3^{\bullet}$	$k = 10^8\ M^{-1}s^{-1}$	(*23*)
33	$> TiCO_3^{\bullet} + TiMLRH \rightarrow TiCO_3^- + > TiMLRH^{\bullet+}$	$k = 10^8\ M^{-1}s^{-1}$	H
34	$> TiCO_3^{\bullet} + TiRR''CH_2 \rightarrow TiCO_3^- + TiRR''CH_2^{\bullet+}$	$k = 10^8\ M^{-1}s^{-1}$	H
35	$> TiCO_3^{\bullet} + > TiRR''CH^{\bullet} \rightarrow TiCO_3^- + TiRR''CH^+$	$k = 10^9\ M^{-1}s^{-1}$	M
36	$> TiOH:\ O_2^{\bullet-} + > TiCO_3^{\bullet} \rightarrow > TiOH:\ O_2 + > TiCO_3^-$	$k = 6.5 \times 10^8\ M^{-1}s^{-1}$	(*11*)
37	$> TiCO_3^{\bullet} + > TiMLR^{\bullet} \rightarrow > TiCO_3^- + > TiMLR^+$	$k = 10^9\ M^{-1}s^{-1}$	M

[a] Refer to Supporting Information for justification of rate constant estimates. H = high confidence − rate constant estimate correct within 1 order of magnitude. M = medium confidence − rate constant estimate may be greater than 1 order of magnitude. L = low confidence/ unknown.

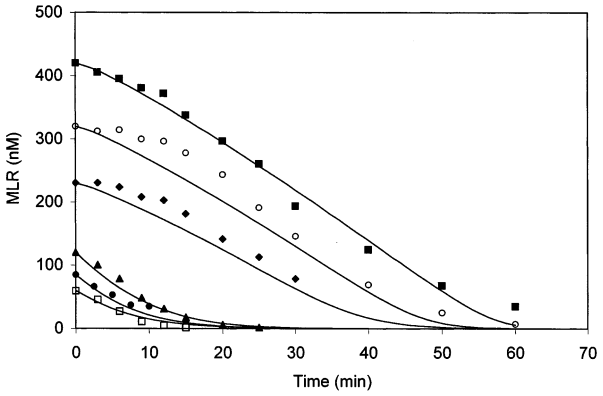

FIGURE 7. Loss of microcystin-LR from solution at pH 3.5 at difference concentrations modeled using model incorporating both surface and solution phase degradation (i.e. degradation model (parts A and B)). Ionic strength of 0.01 M and TiO_2 loading of 1 g·L^{-1}.

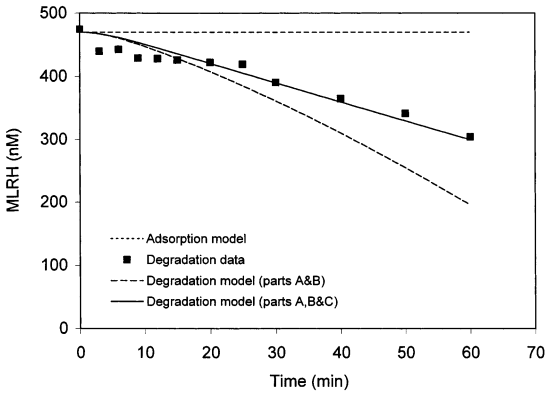

FIGURE 8. Loss of microcystin-LR from solution at pH 8.6 and high concentration. Ionic strength of 0.01 M and TiO_2 loading of 1 g·L^{-1}; "degradation model (parts A and B)" incorporates both surface and solution degradation components; degradation model (parts A, B, and C) includes additional carbonate reactions. Note that at this pH there was no observed adsorption MLRH.

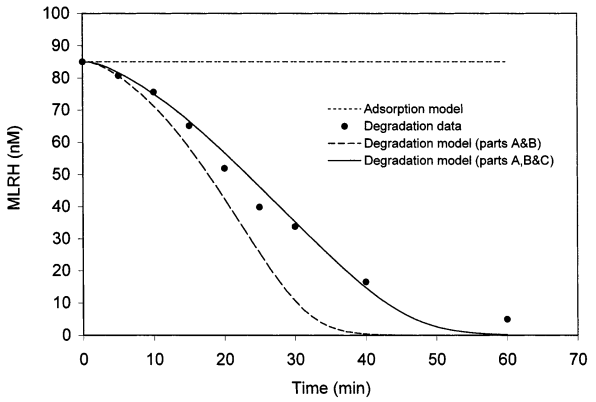

FIGURE 9. Loss of microcystin-LR from solution at pH 8.6 and low concentration. Ionic strength of 0.01 M and TiO_2 loading of 1 g·L^{-1}; "degradation model (parts A and B)" incorporates both surface and solution degradation components; degradation model (parts A, B, and C) includes additional carbonate reactions. Note that at this pH there was no observed adsorption of MLRH.

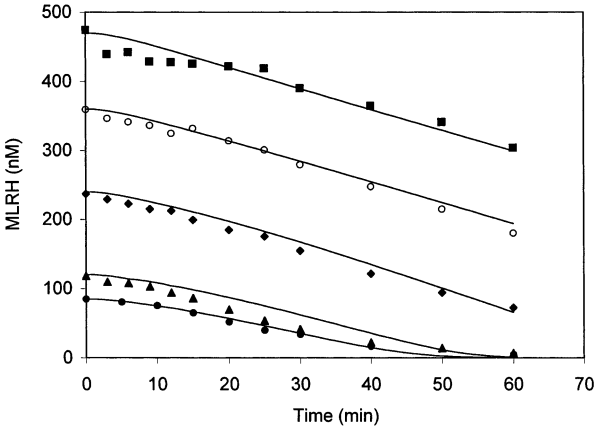

FIGURE 10. Loss of microcystin-LR from solution at pH 8.6 at difference concentrations modeled using surface and solution phase degradation and incorporating carbonate scavenging (i.e. degradation model (parts A, B, and C)). Ionic strength of 0.01 M and TiO_2 loading of 1 g·L^{-1}.

mediated degradation is not responsible for the observed degradation, and, if we consider that hydroxyl radicals do not leave the surface, then the production of organic peroxyl radical via desorption of superoxide as suggested in part B may be an important degradation pathway. The result from application of the model developed for solution phase degradation to the high pH condition is given in Figure 8 (model parts A and B). The only parameters that have been modified from part B are the adsorption and desorption rate constants to account for the observed dependence of adsorption on pH as given in Table 2. While protonated superoxide is no longer the dominant species at high pH, it is assumed that the reactivity of $HO_2^{\bullet-}/O_2^{\bullet-}$ is equivalent. Part B overpredicts the rate of $MLRH^-$ degradation as the model does not consider scavenging and competitive adsorption by bicarbonate. These important pathways clearly need to be included to accurately predict the degradation of $MLRH^-$ at high pH (Table 4). Carbonate is considered to sorb reversibly to TiO_2 surface hydroxy groups (eq 31), and the carbonate complexes are expected to react with other radical species, particularly surface hydroxyl radicals (eq 32). The carbonate radicals generated at the semiconductor surface are expected to either react with other oxidizable species at

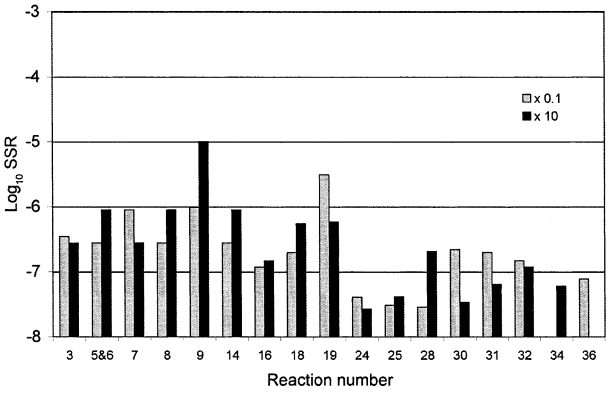

FIGURE 11. Log sum of squares of the residuals (log SSR) for 1 order of magnitude (increase and decrease) perturbation of each rate constant for degradation model (parts A, B, and C) at pH 8.6, C_o = 470 nM, I = 0.01 M, and TiO_2 = 1 g·L^{-1}.

the surface (such as adsorbed $MLRH^-$) or other surface radical species (eqs 33−37).

Inclusion of the carbonate pathways significantly decreases the MLRH degradation rate and provides a good fit over a wide concentration range as shown in Figures 8−10. The model is particularly sensitive to the $O_2^{\bullet-}$ desorption rate (Figure 11; eq 9) and its surface termination with $>TiRR''CH^{\bullet-}$ (Figure 11; eq 19) and to a lesser extent the bulk organic alky radical self-termination (Figure 11; eq 18). This sensitivity indicates the importance of $O_2^{\bullet-}$ surface deactivation and desorption. In a manner similar to the degradation observed for part B, oxygen adsorption/desorption (eq 3) and the production of e^- and h^+ on the surface (eqs 5−8 and 14) are critical as these reactions are responsible for the production and availability of surface $>TiOH:O_2^{\bullet-}$ radicals that may desorb into solution (and subsequently initiate solution phase degradation). The adsorption/desorption of $MLRH^-$ (eq 1) and $RR''CH_2^-$ (eq 2) is no longer a dominant reaction mechanism under high pH conditions as there is no $MLRH^-$ adsorption and more carbonate than $RR''CH_2^-$ adsorbed to the surface. The major effect of carbonate appears not to be through site competition but through the formation of surface carboxyl radicals that deactivate the surface superoxide thereby limiting the amount of superoxide desorption into solution (and subsequent organic peroxyl formation for $MLRH^-$ degradation). The carbonate radicals formed at the surface are anticipated to have relatively short lifetimes, similar to the hydroxyl radicals, and therefore not be a major source of solution phase radicals.

While no independent verification has yet been obtained, the modeling suggests that under conditions of high pH and little to no adsorption of a trace contaminant, degradation of the trace contaminant occurs exclusively in the solution phase through reaction with organic peroxyl radicals. These radicals are produced from the reaction of desorbed superoxide with the bulk organic. Bicarbonate mediation of MLRH degradation appears to occur by adsorption of carbonate onto the titania surface followed by scavenging of surface hydroxyl radicals to form surface carbonate radicals with subsequent rapid quenching of surface bound superoxide. This reduces the quantity of superoxide that desorbs into solution with a resultant reduction in production of organic peroxyl radicals which are the primary agent for trace contaminant degradation in solution.

Acknowledgments

Financial support from DEETYA and Hunter Water Corporation is gratefully acknowledged. Prof Clemens von Sonntag (Max Plank Institute for Radiation Chemistry) is thanked for his helpful comments on superoxide radicals and carbonate.

Supporting Information Available

Modeling approach to surface-mediated degradation (part A), addition of solution phase toxin degradation (part B), and addition of carbonate effects at high pH (part C). This material is available free of charge via the Internet at http://pubs.acs.org.

Literature Cited

(1) Feitz, A. J.; Waite, T. D.; Jones, G. J.; Boyden, B. H.; Orr, P. T. *Environ. Sci. Technol.* **1999**, *33*, 243.
(2) Robertson, P. K. J.; Lawton, L. A.; Munch, B.; Rouzade, J. *Chem. Commun.* **1997**, *4*, 393.
(3) Shepard, G. S.; Stockenström, S.; De Villiers, D.; Engelbrecht, W. J.; Sydenham, E. W.; Thiel, P. G.; Wessels, G. F. S. *Proceedings 4th International Conference TiO_2 Photocatalytic Purification and Treatment of Water and Air*, Albuquerque, New Mexico, 1999.
(4) Lawton, L. A.; Robertson, P. K. J.; Cornish, B. J. P. A.; Jaspars, M. *Environ. Sci. Technol.* **1999**, *33*, 771.
(5) Waite, T. D.; Hug, S.; Feitz, A. J. In *Mineral-Water Interfacial Reactions: Kinetics and Mechanism*; Sparks D. L., Grundl T. J., Eds.; American Chemical Society: Washington, DC, 1999; p 374.
(6) Walsh, K.; Jones, G. J.; Dunstan, R. H. *Phytochemistry* **1997**, *44*, 817−824.
(7) Braun, W.; Herron, J. T.; Kahaner, D. *ACUCHEM Computer Program for Modelling Complex Reaction Systems;* National Bureau of Standards: Gaithersburg, Maryland, 1986.
(8) Braun, W.; Herron, J. T.; Kahaner, D. K. *Intl. J. Chem. Kinetics* **1988**, *20*, 51−62.
(9) Neta, P.; Huie, R. E. Ross, A. B. *J. Phys. Chem. Ref. Data* **1988**, *17*, 1027.
(10) Neta, P.; Huie, R. E.; Ross, A. B. *J. Phys. Chem. Ref. Data* **1990**, *19*, 413.
(11) Bielski, B. H. J.; Cabelli, D. E.; Ardui, R. L. *J. Phys. Chem. Ref. Data* **1985**, *14*, 1041.
(12) Neta, P.; Grodkowski J.; Ross, A. B. *J. Phys. Chem. Ref. Data* **1996**, *25*, 709.
(13) Hoffmann, M. R. Martin, S. T. Choi, W. Bahnemann, D. W. *Chem. Rev.* **1995**, *95*, 69.
(14) Yu, J. C.; Lin, J.; Lo, D.; Lam, S. K. *Langmuir* **2000**, *16*, 7304.
(15) de Lara-Castells, M. P.; Krause. J. L. *J. Chem. Phys.* **2001**, *115*, 4798.
(16) Davis A. P.; Huang, C. P. *Chemosphere* **1993**, *26*, 1119.
(17) Konaka, R.; Kasahara, E.; Dunlap, W. C.; Yamamoto, Y.; Chien, K. C.; Inoue, M. *Free Radical Biol. Med.* **1999**, *27*, 294.
(18) Ishibashi, K.; Fujishima, A.; Watanabe, T.; Hashimoto, K. *Electrochemistry* **2001**, *69*, 160.
(19) Bielski, B. H. J. Cabelli, D. E. In *Active Oxygen in Chemistry*; Foote, C. S., Valentine, J. S., Greenberg, A., Liebman J. F., Eds.; Blackie Academic & Professional: New York, 1995; p 66.
(20) Walling, C. In *Active Oxygen in Chemistry*; Foote, C. S., Valentine, J. S., Greenberg, A., Liebman J. F., Eds.; Blackie Academic & Professional: New York, 1995; p 24.
(21) Bahnemann, D.; Cunningham, J.; Fox, M. A.; Pelizzetti, E.; Pichat, P.; Serpone, N. In *Photocatalytic Treatment of Waters: Aquatic and Surface Photochemistry*; Helz, G. R., Zepp, R. G., Crosby D. G., Eds.; Lewis Publishers: Boca Raton, FL, 1994; p 261.
(22) Kesselman, J. M.; Weres, O.; Lewis, N. S.; Hoffmann, M. R. *J. Phys. Chem. B.* **1997**, *101*, 2637.
(23) Ollis, D. F.; Pelizzetti, E.; Serpone, N. In *Photocatalysis: Fundamentals and Applications*; Serpone, N., Pelizzetti E., Eds.; John Wiley & Sons: New York, 1989; p 603.
(24) Buxton, G. V.; Greenstock, C. L.; Helman, W. P.; Ross, A. B. *J. Phys. Chem. Ref. Data* **1988**, *17*, 513.
(25) Davis, M. J.; Dean, R. T. *Radical-Mediated Protein Oxidation: From Chemistry to Medicine*; Oxford University Press: New York, 1997; p 77.
(26) Ishibashi, K.; Fujishima, A.; Wantanabe, T. Hashimoto, K. *J. Phys. Chem. B* **2000**, *104*, 4934.
(27) von Sonntag, C.; Dowideit, P.; Fang, X.; Mertens, R.; Pan, X.; Schuchmann, M. N.; Schuchmann, H. P. *Water Sci. Tech.* **1997**, *35*, 9.
(28) Goldstein, S. L.; Czapski, G.; Rabani, J. *J. Phys. Chem.* **1994**, *98*, 6586.
(29) Turchi, C.; Ollis, D. F. *J. Catal.* **1990**, *122*, 178.
(30) Cornish, B. J. P. A.; Lawton, L. A.; Roberston, P. K. J. *Appl. Catal. B* **2000**, *25*, 59.

(31) Kormann, C.; Bahnemann, D. W.; Hoffmann, M. R. *Environ. Sci. Technol.* **1991**, *25*, 494.
(32) Nishiwaki-Matsushima, R.; Ohta, T.; Nishiwaki, S.; Suganama, M.; Kohyama, K.; Ishikawa, T.; Carmichael, W. W.; Fuuki, H. *J. Cancer Res. Clin. Oncol.* **1992**, *118*, 420.

Received for review February 22, 2002. Revised manuscript received October 25, 2002. Accepted November 5, 2002.

ES0256010